Radiation-natural convection interactions in partitioned cavities

A. Mezrhab
Faculté des Sciences, Département de Physique, Université Mohamed Premier, Oujda, Morocco, and
L. Bchir
Faculté des Sciences, Université Cadi Ayyad, Marrakech, Morocco

Received November 1997
Revised February 1998
Accepted March 1998

Nomenclature

A = aspect ratio (A = 1)
D = dimensionless thickness of the partition, d/H
Fij = view factors between surfaces Ai, Aj
g = gravitational acceleration
H = enclosure height
k = thermal conductivity
Nucl = local convective Nusselt number
p,P = dimensional and dimensionless pressure
Pr = Prandtl number, ν/α
Ra = Rayleigh number, $g\beta(Th-Tc)H^3/\nu\alpha$
S = dimensionless distance between the partition, s/H
T = temperature
Tc = temperature of the cold wall
Th = temperature of the hot wall
To = mean temperature, (Th + Tc)/2
u,U = dimensional and dimensionless x velocity component
v,V = dimensional and dimensionless y velocity component
W = dimensionless width of the gap, w/H
x,y = Cartesian coordinates
X,Y = dimensionless Cartesian coordinates

Greek symbols

α = thermal diffusivity
β = volumetric expansion coefficient
Θ = dimensionless temperature, T/Th
θ = dimensionless temperature, (T-To)/ΔT
σ = Stefan-Boltzmann constant
ν = kinematic viscosity of the fluid
μ = dynamic viscosity
ε_i = emissivity of the surface Ai
ρo = density of the fluid at T_o
ΔT = maximal difference temperature, $T_h - T_c$

Subscripts

f = refers to the fluid
i = refers to the surface Ai
p = refers to the partition

Introduction

In recent years there have been numerous experimental and theoretical investigations of natural convection in enclosures with partition due to its considerable engineering interest, especially in building applications, for thermal insulation and passive solar heating systems. An excellent review of the past experimental and numerical studies reporting on the flow structures and heat transfer rates in enclosures with partition attached at the top wall and/or at the bottom wall, one extending upwards and the other downwards, can be found in Khan and Yao (1993).

The authors wish to gratefully acknowledge the helpful assistance and discussions provided by Dr Richard Pasquetti (Laboratoire de Mathématiques, Université de Nice, France). His valuable suggestions have stimulated the authors to write the above publication.

International Journal of Numerical Methods for Heat & Fluid Flow
Vol. 8 No. 7, 1998, pp. 781–799.
© MCB University Press, 0961-5539

Not so many research works were done on completely partitioned enclosures and most of them were about vertically divided cavities with very thin partition so that the heat transfer within a partition is essentially one-dimensional (Kelkar and Patankar, 1990; Nakamura and Asko, 1986). A detailed analysis on the effects of a central partition assumed either infinitely thin and isothermal at the average temperature of the hot and cold wall temperatures (ideal partition) or relatively thin was discussed by Karayiannis *et al.* (1992). It is concluded that the heat transfer rate can be calculated using the ideal partition modelling in practical engineering applications concerning air-filled enclosures. The case of multiple vertical partition was studied theoretically and experimentally by Anderson and Bejan (1981) and numerically and experimentally by Nishimura *et al.* (1988). Both works concerned water-filled enclosures and very thin metallic positions.

Probert and Ward (1974) experimentally studied the heat transfer behaviour in a partitioned enclosure of large aspect ratio. They concluded that such a configuration does not produce any significant change in the heat transfer rate across the cavity, even when the partition length equalled 90 per cent of the cavity height, because this arrangement does not greatly disturb the flow. The same problem was reconsidered numerically by Kelkar and Patankar (1990) for air-filled cavity of square cross section. A study was conducted for two Rayleigh numbers (10^5 and 10^6), different widths of the gap connecting the two parts of the enclosure and perfectly conducting or adiabatic thin partition. It was shown that the reduction in heat transfer due to the partition decreases with increasing Ra because of the thinning of the horizontal boundary layers. However, plots of the mean Nusselt number versus the gap width display significant decreases in heat transfer for partition lengths greater than 90 per cent of the height of the cavity, whatever the Rayleigh number and thermal conductivity of the partition. Most recently, the effect of partition conductivity, partition height, partition thickness and partition location on the heat transfer in a two-dimensional square enclosure is reported by Sun and Emery (1994) and Nag *et al.* (1994).

In all of the above-mentioned studies, the influence of radiation is ignored. It can be proved for experimental works in which water or other liquid is used as the working fluid while it is rather surprising that the assumption of neglecting the effect of radiation is not even mentioned in many of the theoretical studies which dealt with complex gas-filled enclosures. For example, the effect of radiation exchanges between surfaces on natural convection is known to be important, even at room temperature, in air-filled cavities the walls of which are not maintained at prescribed temperatures or perfectly reflecting. For partitioned cavities, the radiation-convection interaction to the partition should be considered in a number of practical situations for which the emissivities of the surfaces are generally high. As far as the authors are aware, the paper of Chang *et al.* (1983) is the only one in which interaction of radiation and natural convection was considered for an

enclosure partitioned by two vertical adiabatic partitions of finite-thickness and equal length located at the ceiling and floor. Both surface and gas radiation effects were studied and it is shown that the predominant mechanism by which radiation process increases the overall heat transfer rates is the surface radiation. For the asymptotic case of a completely partitioned cavity, the heat transfer rate by radiation modifies the surface temperatures of the partition, and therefore, the natural convection flow is strongly affected by radiation. A very thin vertical partition located within a rectangular differentially heated cavity acts as a radiation screen. In this case, it is known that approximate analyses based on analogous electrical circuits provide quite accurate estimates of the effect of a radiation screen. An experimental and numerical study on the effect of a partition assumed to be very thin and located at the mid-section of a rectangular cavity was carried out by Nakamura and Asko (1986). It was shown that the emissivities of the top and bottom walls only slightly affect the heat transfer by convection in both cases of conductive and insulated top and bottom walls. On the other hand, the emissivities of the cold and hot walls and of the partition were shown to considerably modify the convective heat transfer.

This paper describes the effect of adding a thick partition located vertically close to the hot wall of a differentially heated cavity, forming a narrow vertical channel in which the flow is controlled by vents at the bottom and top of the partition as shown in Figure 1. A numerical examination of radiation-convection interaction is presented, the focus being on engineering applications at room temperatures and for enclosures filled with air (non-participating gas). It is shown that radiation has a significant influence on the flow and heat transfer in the channel. In this study, the sizes of the vents and thermal conductivity of the partition are other parameters of interest.

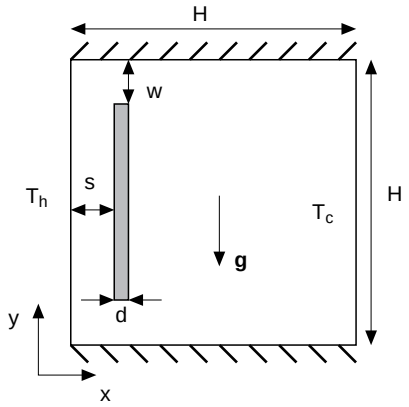

Figure 1.
The geometry considered

Mathematical model

Details of the geometry are shown in Figure 1. The flow is assumed to be incompressible, laminar, steady and two-dimensional in an enclosure of square cross-section, the horizontal end walls are perfectly insulated while the two vertical walls are maintained at two different temperatures T_h and T_c respectively. To simplify the analysis, the Boussinesq approximation is invoked. The working fluid is air and its physical properties except density are assumed to be constant at the average temperature of T_h and T_c . Radiation exchanges in the enclosure are considered to be between opaque, diffuse and gray surfaces.

The equations are nondimensionalized using the following definitions of the dimensionless variables (see the nomenclature):

$$X = x/H \quad ; \quad Y = y/H$$
$$U = uH/\alpha \quad ; \quad V = vH/\alpha$$
$$\theta = (T - T_o)/(T_h - T_c) \quad ; \quad P = (p + \rho_o gy)H^2/\rho_o \alpha^2$$

the dimensionless governing equations in the fluid domain can be expressed as:

Continuity:

$$\frac{\partial U}{\partial X} + \frac{\partial V}{\partial Y} = 0 \tag{1}$$

X momentum :

$$U\frac{\partial U}{\partial X} + V\frac{\partial U}{\partial Y} = -\frac{\partial P}{\partial X} + \lambda Pr\left(\frac{\partial^2 U}{\partial X^2} + \frac{\partial^2 U}{\partial Y^2}\right) \tag{2}$$

Y momentum:

$$U\frac{\partial V}{\partial X} + V\frac{\partial V}{\partial Y} = -\frac{\partial P}{\partial Y} + \lambda Pr\left(\frac{\partial^2 V}{\partial X^2} + \frac{\partial^2 V}{\partial Y^2}\right) + Ra\,Pr\,\theta \tag{3}$$

Energy:

$$U\frac{\partial \theta}{\partial X} + V\frac{\partial \theta}{\partial Y} = R_k\left(\frac{\partial^2 \theta}{\partial X^2} + \frac{\partial^2 \theta}{\partial Y^2}\right) \tag{4}$$

where λ and R_k are equal to 1 in the fluid region and $\lambda = \infty$, $R_k = k_p/k_f$ in the solid region.

The thermal condition at the surface of the partition is determined by a balance between radiation, conduction and convection as

$$R_k\frac{\partial \theta_p}{\partial \vec{n}} = \frac{\partial \theta}{\partial \vec{n}} - N_r\,Q_r \tag{5}$$

where

$$N_r = \frac{\sigma T_h^4}{(k_f \frac{\Delta T}{H})}$$

the radiation number, Q_r the dimensionless net radiative flux and "$\vec{n}$"denotes the unit normal vector to the surface at the partition-air interface.

For the insulated bottom and top walls, the following balance applies:

$$0 = \frac{\partial \theta}{\partial Y} - N_r Q_r \tag{6}$$

The cold and hot walls are maintained at dimensionless temperatures of –0.5 and 0.5 respectively. For the velocity field, the boundary conditions are of the no-slip type.

The equations (5) and (6) are discretized. In order to do this the radiating surface of the solid forming the enclosure and the partition is divided into a number of surfaces A_i, i =1,..., N. Therefore, the dimensionless net radiative flux density along a diffuse gray surface "A_i" is expressed as

$$Q_{r,i} = R_i - H_i \tag{7}$$

where R_i and H_i are the dimensionless radiosity and incident radiation

$$R_i = \varepsilon_i \Theta_i^4 + (1 - \varepsilon_i) H_i \tag{8}$$

where the dimensionless radiative temperature Θ_i is given by

$$\Theta_i = T_i / T_h = [(T_h - T_c)\theta_i + T_o] / T_h \tag{9}$$

For an enclosure consisting of N nonisothermal surfaces such that the radiative properties are uniform over each surface, the radiation flux arriving at surface A_i may be expressed as

$$H_i = \sum_{j=1}^{N} R_j F_{i-j} \tag{10}$$

The diffuse view factor between the two isothermal surfaces, F_{i-j} , depends only on their positions and orientations. For further details on the expression of the net radiative flux, the reader can refer to Siegel and Howell (1972).

The heat flux at the side isothermal walls is the sum of the conductive and radiative fluxes. In dimensionless form, the local heat flux is defined as follows:

$$\frac{q_w}{(k_f \Delta T / H)} = -\left.\frac{\partial \theta}{\partial X}\right|_{X_w, Y} + N_r Q_r(X_w, Y) \tag{11}$$

where $X_w = \{0,1\}$. Therefore, an overall local Nusselt number may be introduced such as

$$Num(X_w, Y) = Nu_c (X_w, Y) + Nu_r (X_w, Y) \quad (12)$$

Where Nu_c and Nu_r are the convective and radiative contributions in Num. The average Nusselt numbers along the side walls are determined as

$$Num(X_w) = \int_0^A \left(-\frac{\partial\theta}{\partial X}\bigg|_{X_w, Y} + Nr\, Q_r (X_w, Y) \right) dY \quad (13)$$

For adiabatic end walls, Num(0) = Num(1).

Finally, the volumetric exchange flow rates through the bottom and top vents which are defined as

$$\psi_{thru} = \int_0^W |U| dY = \int_{A-W}^A |U| dY \quad (14)$$

The solution of these equations is dependent on a large set of parameters. These are Pr, Ra, R_K, A, D, W and S for the conjugate problem without radiation. When including the effect of radiative exchange between surfaces, the above set must be completed by three parameters: Nr, T_o, ε_i . In this paper, the aspect ratio and Prandtl number are set constant (A = 1, Pr = 0.71) and the reference temperature is set to be at T_o = 290K. Furthermore, the geometry and location of the partition wall are defined by D = 0.05 and S = 0.1. Thus, the only geometrical parameter which will be varied in the following is the width of the vents ($0 \le W \le 0.20$).

Numerical procedure

The governing differential equations were solved by a finite-volume method which utilizes a second-order central difference scheme for the advective terms in order to reduce numerical diffusion errors. In the range of Ra numbers investigated, the CDS solution did not exhibit spurious oscillations and the convergence was achieved by using small underrelaxation factors on U, V and θ. The SIMPLER algorithm for pressure-velocity coupling was adopted (Patankar, 1980).The governing equations were cast in transient form and a fully implicit transient differencing scheme was employed as an iterative procedure to reach steady-state. The presence of the partition was accounted by the strategy in which it was characterized by a region of very high viscosity.

The resulting systems of discretized equations were solved by an iterative procedure based on a preconditioned conjugate gradient method. The outer iterative loop was repeated until the following convergence are simultaneously satisfied:

$$\max | \phi^{n+1} - \phi^n | < \varepsilon_\phi \quad (15)$$

Where ϕ is a dependant variable and n the iteration number (i.e. false time step). In most of the cases, the velocity components and temperature were driven to $\varepsilon_u = \varepsilon_v = \varepsilon_\theta < 10^{-6}$. For the pressure correction equation, which is a discretized Poisson equation, the iterative process was stopped when the maximum residual of mass (amount by which the continuity equation was not satisfied) was less than 10^{-8}.

For the combined radiation and convection problem, the surface temperatures on the partition and on the adiabatic end walls were calculated from the non-linear heat balance equation (equations (5) and (6)) by using an inner iterative procedure at every time step for the energy equations. The grid was extended across the adiabatic boundaries by introducing one extra point in order to discretize equations (5) and (6). The surface temperatures were updated from the solution of the energy equation by under-relaxing the boundary evaluation of temperature. At each inner iteration, the linear system of equations for the radiosities was solved by a direct method (Gauss elimination).

The grid was constructed such that the boundaries of the physical domain coincided with the velocity grid lines. The points for pressure and temperature were placed at the center of the scalar volumes. At the fluid-partition interfaces, the control volume faces were also arranged so that a control volume face coincided with an interface. This grid distribution was chosen to ensure the interface energy balance. To avoid a checkboard pressure and velocity fields, staggered grids were used for the U and V-velocity components in the Y and X-directions respectively.

Computation of radiation

Since the radiative properties of the solid surfaces of the enclosure vary from point (even on the isothermal side walls because the incident radiation cannot be assumed as uniform), each of the surfaces was divided into finite number of zones on which the four basic assumptions of the simplified zone analysis was assumed valid. The number of zones retained was determined by the mesh used to solve the differential equations. Therefore, the zoning was nonuniform and the area of each zone varied according to the stretching function and number of grid points used. For N control volume faces, this results in N(N–1)/2 view factors to be calculated and in a linear system of N equations for the radiosities. In view of the meshes used, N was typically of the order of 250. The view factors were determined by using a boundary element approximation (Mezrhab, 1991). This method is summarized here for a two dimensional geometry including shadow effects. Consider two surfaces A_i and A_j, as shown in Figure 2, very long in the direction perpendicular to the plane of the Figure. Let l_i and l_j the lengths of the arcs corresponding to surfaces A_i, A_j in the plane of the Figure. For this 2D-geometry, the view factor between A_i and A_j reduces to :

$$F_{i-j} = \frac{1}{l_i} \int_{l_i} \int_{l_j} \frac{\cos\theta_i \cos\theta_j}{2 r_{ij}} \alpha_{ij} \, dl_i \, dl_j \tag{16}$$

where θ_i (θ_j) is the angle of the outward normal to dl_i (dl_j) with the line $\vec{r}_{ij}$ joining these two elemental surfaces, and α_{ij} a function such as $\alpha_{ij} = 0$ when shadow effects occur or if θ_i (θ_j) $\geq \pi/2$ and $\alpha_{ij} = 1$ otherwise.

The approximation of a length l by boundary elements consists in the discretization of l into elementary surfaces li and approximating each one by a polynomial vector function F(η), where η is curvilinear coordinates associated with the element (Brebbia *et al.*, 1984; Caruso, 1988).

The element is characterized by the degree of a single variable interpolation polynomial and thus the number of interpolation points associated with it as illustrated in Figure 3. The polynomial approximation of the position vector, $\vec{r}(\eta)$, reads:

$$\vec{r}(\eta) = \sum_{p=1}^{P} \varphi_p(\eta) \, \vec{r}_p \tag{17}$$

where $\vec{r}_p$ is the position vector of the point M_p and where $\varphi_p(\eta)$ is the Lagrange's polynomial of degree (P–1) such that:

$$\varphi_p(M_q) = \varphi_p(\eta_q) = \delta_{pq} \tag{18}$$

with δ_{pq} the Kronecker symbol.

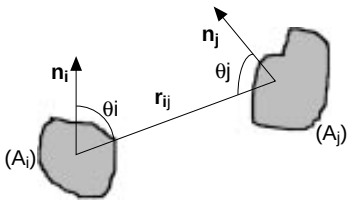

Figure 2.
Radiative exchange between surfaces A_i and A_j

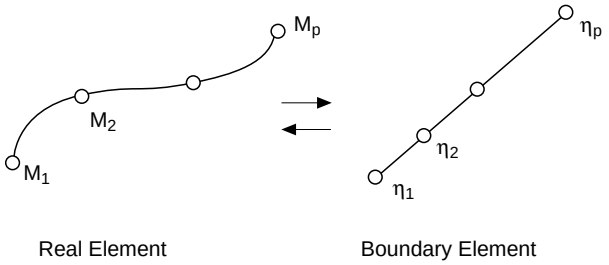

Figure 3.
Curve fitting by boundary elements

The calculation of a curvilinear integral requires the transformation factor :

$$J = \left| \frac{\partial \vec{r}(\eta)}{d\eta} \right| = \left| \sum_{p=1}^{P} \frac{\partial \varphi_p(\eta)}{\partial \eta} \vec{r}_p \right| \tag{19}$$

Using this procedure for the evaluation of the view factor between two boundary elements of length l_i and l_j leads to

$$\cos\theta_i \, dl_i = \frac{(\vec{r}_{ij} \cdot \vec{n}_i)}{|\vec{r}_{ij}|} dl_i = J_i \, d\eta_i \, \frac{\vec{r}_{ij} \cdot \vec{n}_i}{|\vec{r}_{ij}|} \tag{20}$$

Let

$$\vec{G}_i = J_i \vec{n}_i$$

By writing a similar expression for $\cos\theta_j \, dl_j$, we obtain, with $-1 \le \eta \le 1$:

$$F_{ij} = -\frac{1}{l_i} \int_{-1}^{1} \int_{-1}^{1} \frac{(\vec{G}_i \cdot \vec{r}_{ij})(\vec{G}_j \cdot \vec{r}_{ij})}{2 \left| \vec{r}_{ij} \right|^3} \alpha_{ij} \, d\eta_i d\eta_j \tag{21}$$

where

$$l_i = \int_{-1}^{1} \left| \frac{\partial \vec{r}_i}{\partial \eta_i} \right| d\eta_i \tag{22}$$

In the present study, we used rectilinear boundary element and Lagrange polynomials with $\eta_p = 0$ if M_p is at the element center. Therefore, the linear approximation of $\vec{r}_p$ is based on the following polynomials

$$\varphi_1(\eta) = (1 - \eta)/2 \quad ; \quad \varphi_2(\eta) = (1 + \eta)/2 \tag{23}$$

The calculation of the integral is performed by using a Monte Carlo method because this method is well suited for multidimensionnal integration. The algorithm is based on a discretization of the integration domain (square of unit side in two dimensions) into a set of sub-volumes.

In the present study, the partition acts as a screen. The aim is now to produce an efficient algorithm for the calculation of α_{ij} . This algorithm can be explained through Figure 4: the element l_k intercepts the radiation going from a on l_i to b on l_j (see Figure 2) if the quadrilateral abcd is convex. This can be checked by introducing four vectors $\vec{N}_{ab}$, $\vec{N}_{bc}$, $\vec{N}_{cd}$ and $\vec{N}_{da}$ normal to the four sides ab, bc, cd and da. If the element l_k intercepts the radiation from a to b, then:

$$
\begin{aligned}
&(\vec{N}_{ab}.\vec{ac})(\vec{N}_{ab}.\vec{ad}) > 0\\
&(\vec{N}_{bc}.\vec{ba})(\vec{N}_{bc}.\vec{bd}) > 0\\
&(\vec{N}_{cd}.\vec{ca})(\vec{N}_{cd}.\vec{cb}) > 0\\
&(\vec{N}_{da}.\vec{db})(\vec{N}_{da}.\vec{dc}) > 0
\end{aligned}
\qquad (24)
$$

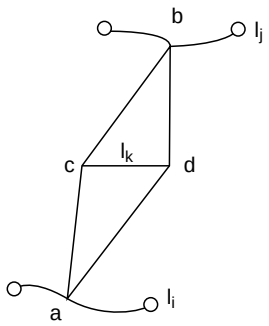

Figure 4.
Radiative exchange between surfaces with screening effects

If three of these requirements are satisfied, then the fourth is satisfied also. When using the Monte Carlo method for calculating the view factors, the points a and b were randomly generated into each of the sub-volumes, until the convergence of the calculation is reached, i.e. until the relative desired accuracy is obtained.

For the present combined convection and radiation problem, the boundary elements were straightforwardly chosen as the N faces of the control volumes lying on the solid surfaces. For each of the boundary elements, the summation rules were checked and it as found that all the view factor summations verified the condition

$$\sum_{j=1}^{N} F_{i-j} = 1 \pm 0.0001.$$

Code validation

The code was extensively exercised on benchmark problems to check its validity. Calculations were first performed for the classical problems of flow in a square driven cavity and for natural convection in differentially heated cavities of various aspect ratios. Next, natural convection in partitioned enclosures was considered. In this section, a comparison of our results with those recently reported by Janssen and Henkes (1993) for natural convection in a square cavity is presented for Ra = 10^6 and 10^8 . Then, the solutions obtained for a square partitioned enclosure are compared with those of Kelkar and Patankar (1990).

Table I allows a comparison of the present results for three quantities selected in Janssen and Henkes (1993): the averaged wall heat transfer Nu along the hot vertical wall, the maximum V_{max} of the vertical along the horizontal velocity along the vertical line through the cavity center. It should be noted that the velocity scales used in Janssen and Henkes (1993) are $(g\beta\Delta T\nu)^{1/3}$ for U and $(g\beta\Delta TH)^{1/2}$ for V. Therefore, the present U and V-velocity components reported in Table I were multiplied by $(Ra\ Pr^2)^{1/3}$ and $(RaPr)^{1/2}$ respectively. As can be seen, all the quantities are in very good agreement with those of Janssen and Henkes (1993). In addition, the deviation with respect to the reference solution of Le Quéré (1991) are very small for the finest grid. We have used the same grid which in the horizontal direction, the stretching function chosen for the U velocities is:

$$X = \frac{i}{i_{max}} - \frac{1}{2\pi}\sin\left(2\pi\frac{i}{i_{max}}\right), \quad i = 0,\ldots,i_{max}$$

where i_{max} refers to the number of grid points in X direction.

In the work of Kelkar and Patankar (1990), the centrosymmetry property of the solution was introduced and the governing equations were solved in half of the physical domain. In the present study, the boundary conditions do not possess symmetry properties due to the radiative heat transfer terms. Therefore, all the computations were carried out on the whole domain, even for the test case discussed in this section. Figure 5 shows the variation of the average Nusselt number and flow rates (equation (14)) with gap width for two Rayleigh numbers and for perfectly conducting partitions as well as for perfectly insulated partitions located in the vertical middle plane of a square, differentially heated cavity. As in Kassemi and Naraghi (1990), we considered very thin partitions. As can be seen in Figure 5, both heat transfer and flow rates decrease with a decreasing gap width. These results can be favourably

Grid	Ra	Num.$Ra^{-1/4}$	V_{max}	U_{max}
Janssen and Henkes				
30×30	10^6	0.2782	0.2658	0.8174
	10^8	0.2977	0.2794	0.8069
60×60	10^6	0.2789	0.2633	0.8145
	10^8	0.3013	0.2647	0.8528
120×120	10^6	0.2790	0.2621	0.8144
	10^8	0.3020	0.2643	0.8769
Present				
30×30	10^6	0.2800	0.2619	0.8179
	10^8	0.3067	0.2601	0.7916
60×60	10^6	0.2792	0.2632	0.8154
	10^8	0.3034	0.2651	0.8520
120×120	10^6	0.2791	0.2626	0.8125
	10^8	0.3025	0.2644	0.8643

Table I.
Comparison of test case with solutions of Janssen and Henkes

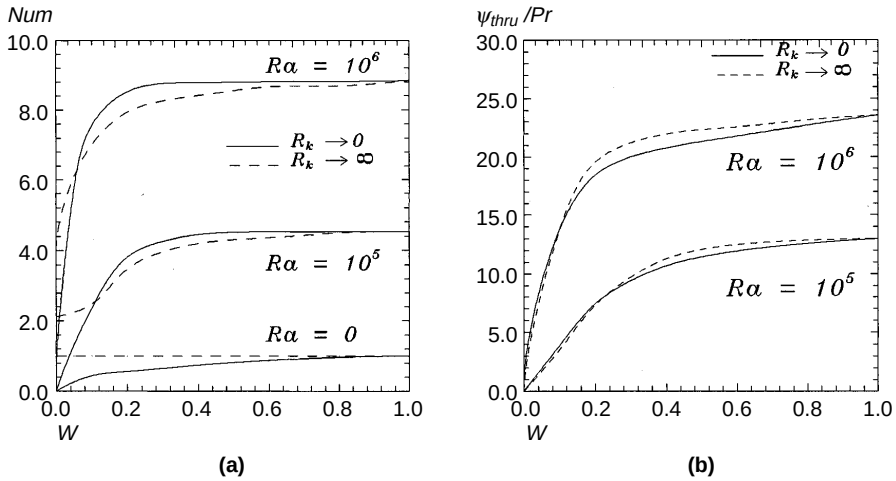

Figure 5.
Variation of: (a) overall Nusselt number, and (b) throughflow strength with gap width for different Rayleigh numbers

compared with those displayed in Figure 2 of Kelkar and Patankar (1990). Despite any numerical data which were reported in Kelkar and Patankar (1990), the largest discrepancies between the present results and those graphically shown in Kelkar and Patankar (1990) can be estimated to be than less 3 per cent.

When we include the radiation, the code was validated with results obtained in Kassemi and Naraghi (1993) for all the cases with the transparent fluid in enclosure. At the same problem, we obtain the same flow and temperature profiles, and the differences between our and published results for the Nusselt number are less than 2 per cent.

Based on the above studies, it was concluded that the code could be reliably applied to the problem under consideration.

Results and discussion

A preliminary study was carried out to determine the optimum nonuniform grid (i.e. the best compromise between accuracy and computational costs). For the calculations reported in this study a 41×41 grid points was chosen to optimise the relation between the accuracy required and the computing time. The grid is nonuniform and is fine near the solid surfaces and tips of the partition. Increasing the number of grid points did not change the results appreciably. For example, adding 20 grid lines in each direction changed the Nusselt number by less than 1 per cent for all values of Ra.

Each case required the specification of seven dimensionless parameters (Ra, Pr, R_k , A, S, D, W) among which the Prandtl number, the cavity aspect ratio, the gap width between the partition and the hot wall and the partition thickness were held fixed at Pr = 0.7, A = 1, S = 0.1 and D = 0.05 respectively. The ranges covered by the remaining parameters were $10^3 \leq Ra \leq 10^8$, $0 \leq W \leq 0.2$ and $0 \leq R_k \leq \infty$. The three dimensionless parameters corresponding to computations of radiation are fixed as: Nr = 30, $\varepsilon_i = 1$ for $1 \leq i \leq N$ and $\Delta T/T_o = 0.12$.

For R_k = 30, W = 0.025 and Ra = 10^6, Figures 6 and 7 show the isotherms and streamlines respectively for Nr = 0 (i.e. in the absence of radiation) and for Nr = 30 (i.e. in the presence of radiation). From the temperature contours, it appears that the radiation heat transfer produces a good homogenization of temperature especially in the cold part of the enclosure : the temperature stratification is less pronounced and the core of the fluid becomes warmer when compared to the natural convection case. It is seen in Figure 8 that the radiation reduces the difference between the top and bottom temperatures. The temperature gradients near the horizontal walls give an indication of the importance of radiative flux. Along a cold wall, the gradients of temperature are less important on the high part of cavity for Nr = 30, than in the low part of cavity. The average convective Nusselt number is also less when we take into account the radiation. One can see also, that the streamlines shown in the case with Nr = 0 are very similar to those including radiation. When Nr = 30, the streamlines indicate that the central vortices becomes weaker. Note, however, that the flow near the cold wall remains strong in order to dissipate

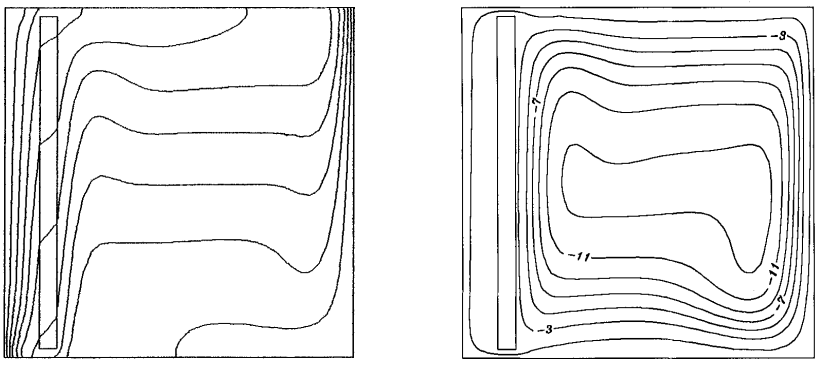

Figure 6.
(a) isotherms and (b) streamlines for Ra = 10^6, W = 0.025, Nr = 0

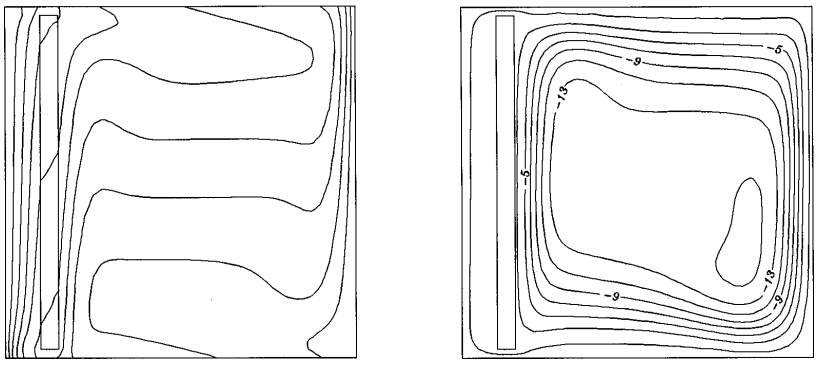

Figure 7.
(a) isotherms and (b) streamlines for Ra = 10^6, W = 0.025, Nr = 30

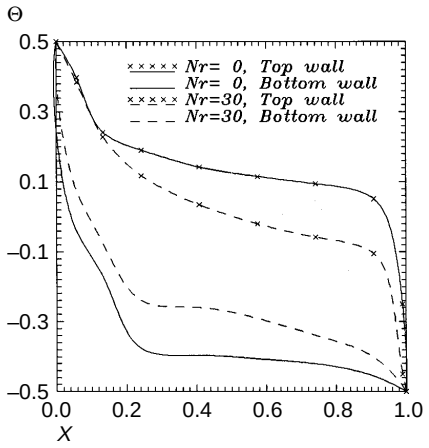

Figure 8.
Wall temperature distribution for Ra = 10^6, W = 0.025

the extra heat delivered by radiation into the cold sink. It is observed that the radiation effects increase the vertical velocity near the cold wall by 5 per cent. This is due to the increase of the flow rate through the bottom and the top vents. As a matter of fact, the difference between the average fluid temperatures in the left part and the right part of cavity increases with radiation, the circulation increases in the channel delimited by the hot wall and the partition.

Nusselt number

The effect of the width of the vents on heat transfer rate was first examined for R_k = 30 (i.e. $k_p \cong 1$ W/m.K) for various Ra. Figure 9 shows that the presence of the partition has a significant influence on Num provided W < 0.1. The effect of W on the Nusselt number is weaker until Ra = 10^4 because the circulation of

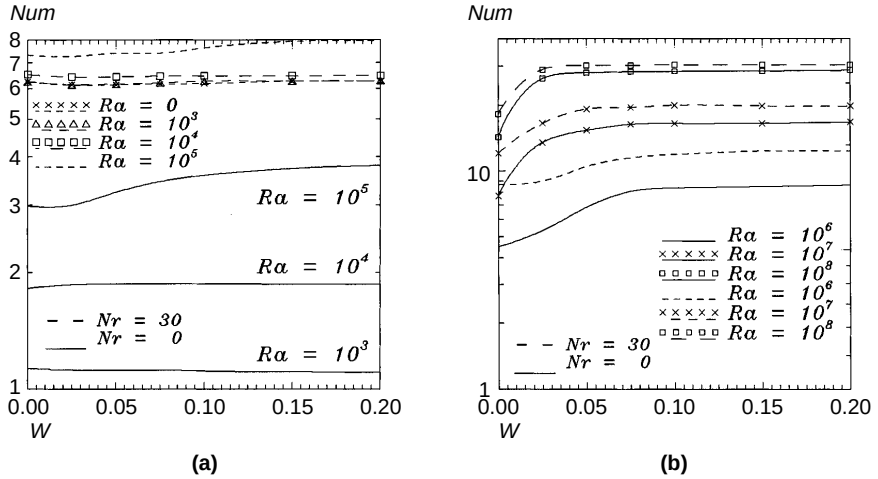

Figure 9.
Variation of overall Nusselt number with W, (a) for Ra ≤ 10^5, (b) for 10^6 ≤ Ra ≤ 10^8

air is weak, thus the conduction is the principal mode of heat transfer. It is observed that there is an increasing of Num with W for $W \leq 0.1$ and $Ra \leq 10^6$, it is the same for $W \leq 0.05$ and $Ra \geq 10^7$. The radiation increases the overall average Nusselt number for all values of W and Ra, however, this increasing is less pronounced as Ra is high. For example, for Nr = 30, the effect of radiation is to multiply Num by 6 if Ra = 0, and by 2 if $Ra = 10^5$ whereas the increasing is only in the order of 7 per cent for $Ra = 10^8$. For all simulations which correspond to Figure 9, the radiative Nusselt number Nu_r on the hot wall comprises between 3 and 4.5. Consequently, the radiative contribution in combined heat transfer becomes weaker and weaker as Ra increase.

The variation of the convective portion in local Nusselt number on the hot wall, Nucl = $Nu_c(0,Y)$, is shown in Figure 10. It can be seen that the radiation increases Nucl in the bottom portion near the hot wall for $Ra = 10^5$ and decreases Nucl for $Ra = 10^8$. This is explained one more time by the throughflow strength which is much more important at moderate Ra. At high Ra, the circulation induced by the buoyancy force is important and the principal effect of radiation is also to reduce the convective heat transfer on the hot wall (the same throughflow like two hot surfaces instead of one surface).

Throughflow strength

Figure 11 shows the variation of ψ_{thru} with W for $10^5 \leq Ra \leq 10^8$. For $Ra \leq 10^4$, ψ_{thru} is smaller even if it increases under the radiation effect, and its maximal value is about 0.3 when the width of the vents is inferior at 0.2. At $Ra = 10^5$, the radiation effect on the ψ_{thru} is significant from $W \geq 0.15$; we can also note an increasing in the order of 8 per cent. For W = 0.025, the increasing of ψ_{thru} under the effect radiation begins from $Ra \geq 10^7$.

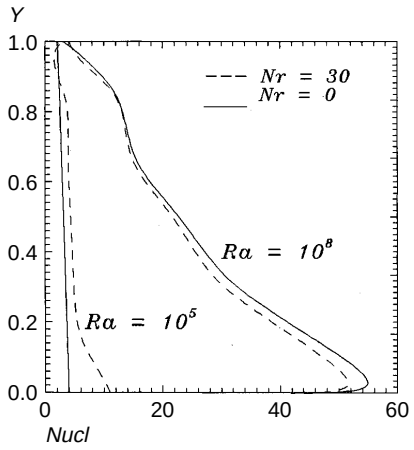

Figure 10.
Effect of radiation on convection portion in local Nusselt number

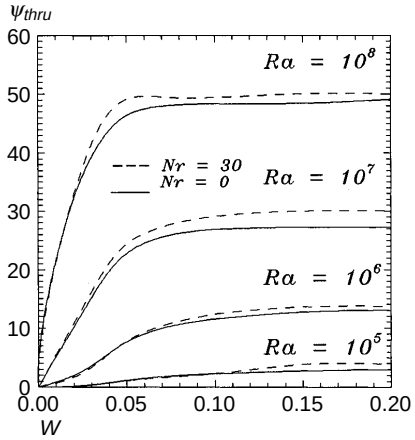

Figure 11.
Variation of throughflow strength with W

Effect of partition conductivity

The computations were carried out for two dimensionless conductivity ratios (R_k = 0 and ∞) and for a fixed width of the vents (W = 0.025). The results obtained for R_k = ∞ are similar to those obtained for R_k = 30. The effect of partition conductivity on the Nusselt number is shown in Figure 12 for Nr = 0 and Nr = 30.

When R_k = 0, the value of the Nusselt number is weak for Ra ≤ 10^5 because the fluid gets hot due to its inability to transfer heat through the adiabatic wall. Otherwise, the heat transfer from the hot wall to the cold wall is made by the vents and, since W is small, the flow is only generated if Ra ≥ 10^5. (For W = 0, we have obviously Num = 0 for all values of Ra). When Ra ≥ 10^5, the transferred heat flux increases rapidly and for Ra = 10^8, the partition does not decrease practically the heat transfer. If we take into account the radiation, we observe that the transferred radiative flux is small due to the obstacle played

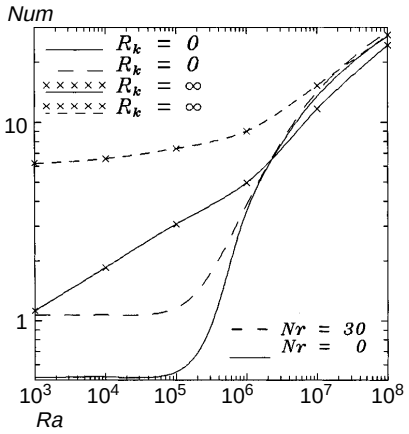

Figure 12.
Effect of partition conductivity on the Nusselt number

by the partition. The order of its contribution in the Nusselt number is 50 per cent on the hot wall for Ra = 10^5. It decreases when Ra increases and is just only 10 per cent at Ra = 10^8 . The variation of the local convective Nusselt number along the hot wall (Figure 13) confirms the strong obstacle effect played by the partition at Ra = 10^5 and its weaker influence at Ra = 10^8. It is shown too that the convective contribution in the overall average Nusselt number is, in this case, slightly modified by the radiation.

When $R_k = \infty$, the isolating effect of the partition is less important; however, the rubble effect on the circulation of the fluid is reinforced. We have also Num ≥ 1 for all values of Ra. It can be explained easily: if the Rayleigh number is very small in order that the fluid circulates between the hot wall and the partition, the heat is transferred by conduction in the fluid lame and the partition. The problem is also similar to the one of the cavity differentially heated with a thermal resistance on the hot wall. When Ra increases, we observe that the overall average Nusselt number becomes almost independent of the partition conductivity from Ra $\cong 2.10^6$. It is, however, slightly inferior at the one obtained for $R_k = 0$. It is due to the fact that the circulation of the fluid is made essentially in the cold part of the cavity, the aspiration effect is also weaker than for $R_k = 0$. Finally, though the nature of flow is sensibly affected by the value of the partition conductivity, the heat flux transferred at high Rayleigh number (Ra $\cong 10^8$) is almost independent of the partition conductivity, of the exchange by radiation and of the width of the vents when the one is superior at 2.5 per cent of the height of the cavity. The calculations of the throughflow through the vents and the velocity profile confirms this commentary made in Figure 12.

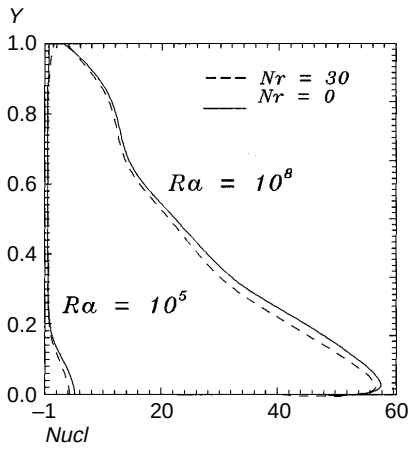

Figure 13
Variation of local convective Nusselt number along the hot wall for $R_k = 0$

Conclusions

A numerical study of natural convection and radiation in partitioned square enclosure, differentially heated, has been presented. Within the investigated parameter ranges, the following conclusions can be drawn :

- For all values of Ra, the effect of the partition may be negligible if the width of the vents is superior at W = 0.1.
- For a given value of W, the effect of the partition becomes negligible when Ra is high.
- The radiation standardizes the temperatures in the two parts of the cavity and increases the difference between the average temperatures, increases the rate of the fluid in the space delimited by the wall and the partition (channel effect). Its effect is to increase the circulation in all the enclosure.
- Our study was carried out with parameter radiation Nr = 30, which corresponds to moderate difference temperature between the hot and the cold wall. However, we have observed that the radiation plays a very important role in the overall heat transfer and the one is enhanced significantly if the radiation is included.

References

Anderson, R. and Bejan, A. (1981), "Heat transfer through single and double vertical walls in natural convection: theory and experiment", *International Journal Heat Mass Transfer,* Vol. 24 No. 10, pp. 1611-20.

Brebbia, C.A., Telles, J.C.F. and Wrobel, L.C. (1984), *Boundary Element Techniques,* Springer-Verlag.

Caruso, A. (1988), "Application de la méthode des éléments de frontière à la modélisation des transferts de chaleur par diffusion thermique", thèse de Doctorat de l'Université de Provence, Marseille.

Chang, L.C., Yang, K.T. and Lloyd, J.R. (1983), "Radiation-natural convection interactions in two dimensional complex enclosures", *Journal of Heat Transfer*, Vol. 105, pp. 89-95.

Janssen, R.J.A. and Henkes, R.A.W.M. (1993), "Accuracy of finite-volume discretizations for the bifurcating natural-convection flow in a square cavity", *Numerical Heat Transfer*, Part B, Vol. 24, pp. 191-207.

Karayiannis, T.G., Ciofalo, M. and Barbaro, G. (1992), "On natural convection in a single and two zone rectangular enclosure", *International Journal Heat Mass Transfer*, Vol. 35 No. 7, pp. 1645-57.

Kassemi, M. and Naraghi, M.H.N. (1993), "Analysis of radiation-natural convection interactions in 1-g and low-g environments using the discrete exchange factor method", *International Journal of Heat Mass Transfer*, Vol. 36 No. 17, pp. 4141-9.

Kelkar, K.M. and Patankar, S.V. (1990), "Numerical prediction of natural convection in square partitioned enclosures", *Numerical Heat Transfer,* Part A, Vol. 17, pp. 269-85.

Khan, J.A. and Yao, G.F. (1993), "Comparison of natural convection of water and air in a partitioned rectangular enclosure", *International Journal Heat Mass Transfer,* Vol. 36 No. 12, pp. 3107-17.

Le Quéré, P. (1991), "Accurate solutions to the square thermally driven cavity at high Rayleigh number", *Computers & Fluids,* Vol. 20, pp. 29-41.

Mezrhab, A. (1991), "Contribution à l'étude numérique et expérimentale des échanges radiatifs", thèse de Doctorat de l'Université de Provence, Marseille.

Nag, A., Sarkar, A. and Sastri, V.M.K. (1994), "Effect of thick horizontal partial partition attached to one of the active walls of a differentially heated square cavity", *Numerical Heat Transfer*, Part A, Vol. 25, pp. 611-25.

Nakamura, H. and Asko, Y. (1986), "Combined free convection and radiation heat transfer in rectangular cavities with a partition wall", *Heat Transfer Japanese Research*, pp. 60-81.

Nishimura, T., Shirashi, M., Nagasawa, F. and Kawamura, Y. (1988), "Natural convection heat transfer in enclosures with multiple vertical partitions", *International Journal Heat Mass Transfer,* Vol. 31 No. 8, pp. 1679-86.

Patankar, S.V. (1980), *Numerical Heat Transfer and Fluid Flow,* McGraw-Hill, New York, NY.

Probert, S.D. and Ward, J. (1974), "Improvements in the thermal resistance of vertical, air-filled, enclosed cavities", *Proc. 5th International Heat Transfer Conf.,* Tokyo, NC 3.9, pp. 124-8.

Siegel, R. and Howel, J.R. (1972), *Thermal Radiation Heat Transfer,* McGraw-Hill, New York, NY.

Sun, Y.S. and Emery, A.F. (1994), "Multigrid computation of natural convection in enclosures with a conductive baffle", *Numerical Heat Transfer,* Part A, Vol. 25, pp. 575-92.